Combined Measurement of Directional Raman Scattering and Surface-Plasmon-Polariton Cone from Adsorbates on Smooth Planar Gold Surfaces

Charles K. A. Nyamekye, [a, b] Stephen C. Weibel, [c] Jonathan M. Bobbitt [a, b] and Emily A. Smith [* a, b]

[a] The Ames Laboratory, U.S. Department of Energy, Ames, Iowa 50011, United States

[b] Department of Chemistry, Iowa State University, Ames, Iowa 50011, United States

[c] Surface Photonics Inc., Madison, Wisconsin 53719, United States

[*] Corresponding Author (esmith1@iastate.edu, 1-515-294-1424)

ORCID ID
Charles K. A. Nyamekye: 0000-0002-5190-3213
Stephen C. Weibel: 0000-0002-5910-9671
Jonathan M. Bobbitt: 0000-0003-4639-1038
Emily A. Smith: 0000-0001-7438-7808

Abstract

Directional-surface-plasmon-coupled Raman scattering (directional RS) has the combined benefits of surface plasmon resonance and Raman spectroscopy, and provides the ability to measure adsorption and monolayer-sensitive chemical information. Directional RS is performed by optically coupling a 50-nm gold film to a Weierstrass prism in the Kretschmann configuration and scanning the angle of the incident laser under total internal reflection. The collected parameters on the prism side of the interface include a full surface-plasmon-polariton cone and the full Raman signal radiating from the cone as a function of incident angle. An instrument for performing directional RS and a quantitative study of the instrumental parameters are herein reported. To test the sensitivity and quantify the instrument parameters, self-assembled monolayers and 10 to 100-nm polymer films are studied. The signals are found to be well-modeled by two calculated angle-dependent parameters: three-dimensional finite-difference time-domain calculations of the electric field generated in the sample layer and projected to the far-field, and Fresnel calculations of the reflected light intensity. This is the first report of the quantitative study of the full surface-plasmon-polariton cone intensity, cone diameter, and directional Raman signal as a function of incident angle. We propose that directional RS is a viable alternative to surface plasmon resonance when added chemical information is beneficial.

Introduction

For several decades, surface plasmon resonance (SPR) has been studied extensively for a range of applications, such as detecting and monitoring the kinetics, affinity, and selectivity of interactions between an adsorbate and an immobilized binding partner.[1-7] A drawback to SPR is the encoded signal provides minimal, at best, information about what is adsorbed at the surface; what information is provided is typically through a series of control experiments to measure nonspecific binding.[8] Under

total internal reflection, surface plasmons can be generated when the excitation light is at an appropriate incident angle upon a high refractive index prism traveling to an interface with a thin noble metal film and an adjacent dielectric material with a lower refractive index. An exponentially decaying evanescent wave is generated in the dielectric material that extends from ~100 nm to ~2 μm, depending on the excitation wavelength and the indices of refraction of the interfacial media.[9-12] In contrast, on the prism side, excitation of surface plasmons in the plane of the metal film (in-coupling) and scattered light through the prism (out-coupling) results in a hollow cone of directional emission at a sharply defined angle.[13-18] This is referred to as the surface-plasmon-polariton cone (or more simply "cone"). An illustration of the cone generated using a Weierstrass prism in the Kretschmann geometry is shown in Fig. 1. Braundmeier *et al.*[19] proposed two mechanisms for the generation of the cone they measured using a 40-nm silver film: (1) momentum conserving optical coupling and (2) scattering from surface irregularities (e.g., grain boundaries and dislocations) or roughness coupling. The angle of incidence (θ_{inc}) that results in the emission cone is given by equation 1, where η is the refractive index of the prism and ϵ is the dielectric function of the metal film.[19]

$$\theta_{inc} = arcsin\left[\eta^{-1}\left(\frac{\epsilon}{1+\epsilon}\right)^{\frac{1}{2}}\right] \qquad (1)$$

Fluorophores in close proximity to a gold or silver surface can be excited within the cone and this is referred to as surface plasmon coupled emission.[20-24] Gryczynski *et al.*[25, 26] reported the surface plasmon coupled emission from 30 to 750-nm polyvinyl alcohol films with incorporated fluorescent sulforhodamine 101 on a 50-nm silver substrate. They photographed the surface plasmon coupled emission cone projected onto tracing paper, and concluded that there was an increase in the angle where the maximum luminescence was measured with increasing polyvinyl alcohol thickness. Also, four surface plasmon coupled emission cones were observed for a 745-nm film, but quantification of the cone parameters was not reported. Quenching and photobleaching of the fluorophores is a concern with luminescence,[27] and more importantly, chemical identification of the adsorbates is limited using luminescence.

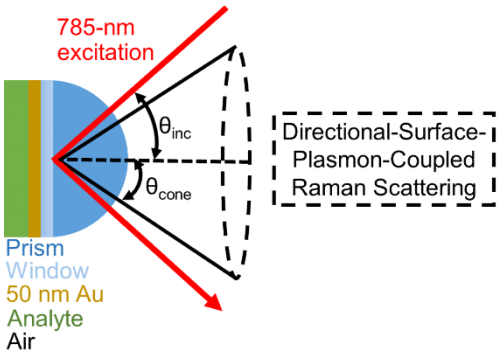

Fig. 1 Schematic illustrating the Weierstrass prism (formed by optically coupling a sapphire hemispherical prism to a sapphire window) in the Kretschmann configuration with a 50-nm thick gold substrate. The signals are collected on the *prism side* (i.e., with collection optics on the right side of this schematic). The data include an image of the full cone to extract the intensity and diameter as well as Raman scattering as a function of incident angle. The signal on the *sample side* refers to placing the collection optics on the left side of this schematic. The schematic is not drawn to scale.

Directional-surface-plasmon-coupled Raman scattering (directional RS) generated within the cone has also been demonstrated, with some of the earliest reports from Furtak,[28] Otto,[18] and Futamata.[29] In 1990, Byahut and Furtak[28] used a device that allowed the collection of the Raman signal from the entire cone. In their set-up, a hemispherical prism and a paraboloid mirror in the Kretschmann configuration was used to obtain a Raman spectrum of a paranitrosodimethylaniline monolayer on a silver film. A Weierstrass prism is capable of collecting the entire cone in the Kretschmann and Otto configurations.[18, 30, 31] Futamata *et al.*[29, 30, 32] projected the entire cone onto paper from an attenuated total reflection device in the Otto configuration (Weierstrass prism/air gap/adsorbate/silver). By controlling the thickness of the air gap and/or placing water in the air gap, the Raman band intensities were increased for monolayers of copper-phthalocyanine, p-nitrothiophenol and p-aminothiophenol with 514.5-nm excitation. However, in all these fundamental studies, the cone was projected onto paper in a manner that did not facilitate the quantification of the cone parameters, or was not recorded at all, thus the ability to extract optical information about the adsorbed analytes was not demonstrated.

Li *et al.*[33] collected the Raman spectrum of p-aminothiophenol on a silver substrate coupled to a semi-cylindrical prism on an angle-resolved Raman spectrometer with 532-nm excitation. Etchegoin *et al.*[34, 35] were able to simultaneously measure the SPR reflectivity and Raman signal of a monolayer of Nile Blue on 50-nm silver and gold films as a function of the incident angle. While Li *et al.* and Etchegoin *et al.* collected the Raman signal as a function of incident angle, they did not study the surface-plasmon-polariton cone nor collect the Raman signal from the entire cone (thus the signal collection was not optimized).

When an appropriately *roughened* metal film replaces the smooth noble metal film, surface enhanced Raman spectroscopy (SERS) can be combined with directional RS. Huo *et al.*[36] demonstrated directional RS with SERS in the reverse Kretschmann configuration (illumination from the sample side). They measured 4-aminothiophenol adsorbed on a silver nanoparticle-on-film SERS substrate, although they did not show an image of the cone nor collect the SERS signal from the entire cone. SERS substrates enhance the Raman signal, but SERS generally precludes the measurement of smooth films, and the signal is not simply modelled by calculated parameters.

While neither the surface-plasmon-polariton cone nor Raman scattering generated from the cone are new concepts, only a handful of reports[28-32] have shown the optimized collection of the entire Raman signal from the cone with the ability to scan over a limited range of the incident angles, but the ability to quantify the properties of the cone as a function of adsorption and incident angle have not been previously reported. Herein we show for the first time: (1) an instrument capable of collecting the full cone and the full Raman scattering signal emanating from the cone as functions of incident angle, which could be a useful alternative to SPR. In order to fulfill this potential, we show: (2) that the Raman signal has monolayer sensitivity on a smooth film, (3) the first quantification of the cone intensity and diameter as a function of incident angle for varying adsorbate layers, and we demonstrate (4) that it is possible to model all the instrument parameters through simple calculations to extract sample information from these properties.

The directional RS signal using a smooth planar gold film is enhanced relative to measuring the same number of molecules in solution by Raman spectroscopy. This is the result of the enhanced electric field that is produced at the interface under total internal reflection.[9] In addition, the presented instrumentation enables the full Raman signal from the cone to be collected, further increasing the signal compared to studies where only a portion of the directional Raman signal was collected. The

larger signal enables the measurement of monolayers without the use of a SERS substrate, so smooth films can be measured and it is straight forward to model the signals with finite-difference time-domain and Fresnel calculations. Furthermore, the multidimensionality of the data (cone diameter and intensity and Raman scattering as a function of incident angle) provides the ability to measure more sample properties compared to either SPR or Raman scattering techniques alone. This is highlighted by our related previous work using a technique called scanning angle Raman spectroscopy,[37-45] whereby the incident light is scanned over a wide range of angles while simultaneously collecting the reflected light from the prism side and Raman scattering on the sample side of the interface. Scanning angle Raman spectroscopy (in the absence of a gold film) was used to identify buried interfaces in a multi-layered system with ~10s of nanometer spatial resolution. This new directional RS instrument and methodology reported herein can be applied to study numerous smooth thin films including sensors, organic solar cells, and more generally as an alternative to surface plasmon resonance spectroscopy when added chemical information is beneficial.

Experimental

Materials

Thiophenol (assay 99%, CAS# 108-98-5), poly(bisphenol A carbonate) (M_w = 64,000, CAS# 25037-45-0), polystyrene pellets (M_W = 192,000, CAS# 9003-53-6), 200 proof ethanol (assay 99.5%, CAS# 64-17-5), and sulfuric acid (assay 99.999%, CAS# 7664-93-9) were purchased from Sigma-Aldrich (St. Louis, MO) and used as received. Methylene chloride (assay 99.9%, CAS# 75-09-2), anhydrous toluene (assay 99.8%, CAS# 108-88-3), and hydrogen peroxide (assay 31.7%, CAS# 7722-84-1) were purchased from Fisher Chemical (Pittsburgh, PA). Deionized water from an 18.2 MΩ cm^{-1} EasyPure II filtration system (Thermo Scientific, Waltham, MA) was used as a rinsing solution.

Sample Fabrication

The sample configuration consisted of a sapphire Weierstrass prism (Fig. 1, ISP Optics Irvington, NY) optically coupled to a 25.4 mm diameter sapphire substrate (Meller Optics, Providence, RI) containing a 2-nm titanium (99.999% pure Ti) adhesive layer and a 50-nm gold (99.999% pure Au) layer (metal deposition by Platypus Technologies LLC., Madison, WI). The optical coupling of the prism to the sapphire substrate used a η_D = 1.7400 index matching fluid (Cargille Laboratories Inc., Cedar Grove, NJ) to ensure optical contact without the presence of air gaps. Before preparing the thin films, the gold substrate was cleaned with piranha solution (3:1 mixture of sulfuric acid and hydrogen peroxide) for 5 minutes inside a fume hood (NOTE: piranha solution may result in chemical and thermal burns if not handled with extreme caution). The gold substrate was rinsed with deionized water, then immersed in a 50:50 (v/v) ethanol and deionized water bath for sonication using an ultrasonic cleaner for 10 minutes. Then the cleaned gold substrate was dried with a stream of N_2 gas. To form a self-assembled monolayer of thiophenol, the clean gold substrate was immersed in an ethanoic 10 mM thiophenol solution for 24 hours. The monolayer sample was rinsed with ethanol and dried with a stream of N_2 gas. For the polymer samples, solutions of poly(bisphenol A carbonate) in methylene chloride and solutions of polystyrene in toluene were prepared with concentrations ranging from 0.001 to 1.0 g mL^{-1}. To make the polymer films, 200 µL of solution was spin-coated on the gold substrate at 3000 rpm for one minute

using a KW-4A spin coater (Chemat Technology, Inc. Northbridge, CA). The polymer film was allowed to dry in ambient conditions overnight. The thickness of poly(bisphenol A carbonate) and polystyrene was measured with an AlphaStep® D-600 stylus profiler (KLA-Tencor Corp. Milpitas, California). A calibration curve of thickness versus solution concentration was generated and used to fabricate polymer films approximately 10 and 50 nm thick poly(bisphenol A carbonate) and 30, 60, 70, 80, 90, and 100 nm thick polystyrene. The exact thickness of each film was subsequently measured with profilometry (ESI Fig. S1) after the surface-plasmon-polariton cone and Raman data were collected. For simplicity, the samples will be referred to by their approximate thickness throughout the text.

Directional-surface-plasmon-coupled Raman Spectrometer

A schematic of the instrument is shown in Fig. 2. A sample holder was designed to secure the prism and the gold substrate onto the instrument. A 785-nm near-infrared diode laser (Toptica Photonics XTRA II, Victor, NY) with a power of 200 mW measured after FL1 was directed at the prism. A linear polarizer and half-wave plate were used to ensure p-polarized light was incident upon the interface, and a laser line filter was used to clean up the laser profile. The laser beam was directed with mirrors M1 and M2 while translation mirror TM1 was used to control the incident angle. The speed of the translational mirrors can be varied. For this work, the slowest setting on the stage movement was utilized. It is noteworthy that the use of a translational mirror to control the incident angle has the potential to reduce acquisition times compared to the use of a rotational stage. The laser light was directed onto the sample by FL2, an aspherical lens (50 mm focal length and 75 mm diameter). The beam was 250 µm in diameter at the air/prism interface. TM2 was used to block the reflected light from reaching the detector.

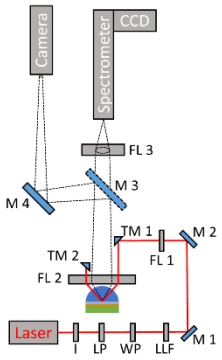

Fig. 2 Instrument schematic from the top of the 785-nm excitation directional-surface-plasmon-coupled Raman spectrometer. I: iris, LP: linear polarizer, WP: waveplate (λ/2), LLF: laser line filter, M: mirror, FL: focusing lens, TM: translation mirror, CCD: charge-coupled device. M3 can be flipped down to collect the Raman signal.

Surface-plasmon-polariton Cone Measurements

An image of the cone (i.e., directional Rayleigh signal) was collected with M3 in the light path directing it to M4 and a 75 mm (f/1.3) Kameratori TV Lens (Tampere, Finland) attached to an 11.340 mm × 7.130 mm, 2.32 mega pixel CMOS sensor (IDS Imaging Development Systems GmbH, Obersulm,

Germany). Cone images were acquired using software that was integrated with a stepper motor for varying the incident angle of the laser excitation. For the cone intensity measurements, the incident angle range was 0.00° to 60.00° with an angle resolution of 0.06°. The capability of the instrument to image the cone while scanning the incident angle of light for a Weierstrass prism/50-nm thick gold substrate/air interface in the Kretschmann configuration is shown in ESI Fig. S2 and accompanying movie. All images of the cone were collected with a fixed distance between FL2 and the camera.

Directional-surface-plasmon-coupled Raman Measurements

When M3 was out of the light path, the Raman signal emanating from the full cone was collected on the prism side. The cone of Rayleigh scattering was visualized using an infrared card, confirming the collection of the entire cone. FL3 was a N-BK7 plano-convex lens, (75 mm diameter, 100 mm focal length, Thor Laboratories, Newton, NJ), which was used to focus the light onto a Kaiser HoloSpec Raman spectrometer (Kaiser Optical Systems, Inc. Ann Arbor, MI) with a 100 μm slit and a HSG-785-LF volume phase holographic grating. The detector was a Princeton Instruments (Trenton, NJ) PIXIS 400 1340 × 400 near-infrared-enhanced charged-coupled device (CCD) with 20 μm × 20 μm pixels controlled with the Princeton Instruments WinSpec/32 [v.2.6.14 (2013)] software. The detector was thermoelectrically cooled to -70 °C. Due to efficiency limitations of the instrument components, there is invariably some loss of the Raman scattering prior to detecting the final signal. A solution of acetonitrile-toluene was used for wavelength calibration. Raman data were collected from 34.0° to 54.0° using a 0.2° angle resolution, except within ± 1° of the angle producing the maximum intensity where an angle resolution of 0.06° was used. For the thiophenol monolayer, an acquisition time of 10 s and 3 accumulations was sufficient to obtain a high signal-to-noise ratio spectrum. The Raman spectra of 10 and 50-nm poly(bisphenol A carbonate) were obtained with 180 s and 120 s acquisition times, respectively. For the polystyrene films, the Raman spectra of the 70, 80, 90, and 100-nm were obtained with a 30 s acquisition time and 120 s for the 30 and 60-nm polystyrene films. All spectra of the polymer films used 2 accumulations to facilitate cosmic ray removal. All spectra were collected at room temperature. Three replicates experiments were obtained by taking consecutive scans through the entire incident angle range.

Data Analysis and Calculations

All calculations assumed that all layers have a constant index of refraction for p-polarized 785-nm excitation and were homogeneous. The input parameters were the indices of refraction and thickness of each layer shown in Fig. 1. The input refractive indices of sapphire, poly(bisphenol A carbonate), polystyrene, thiophenol, air, and gold at 785 nm were 1.762, 1.571, 1.578, 1.568, 1.000, and 0.10219 (η_{Au}) and 5.0998 (k_{Au}), respectively. The thicknesses of the prism and air layers were semi-infinite compared to the polymer (10 to 100 nm) and the gold (50 nm) layers.

Calculations to model the surface-plasmon-polariton cone were performed using three-dimensional finite-difference time-domain simulations (EM Explorer, San Francisco, CA). The calculated emission cone diameter was obtained from the tangent of the far-field angular radiation pattern depicting the directionality of the scattered light on the prism side and the distance between the prism and the detector as experimentally measured for the instrument shown in Fig. 2. The CMOS camera used to measure the cone was calibrated with a metal ruler placed across the planar side of the

collection lens (FL2). An image of the metal ruler was acquired and the ruler scale was used to generate a distance per pixel calibration for the CMOS image. The stated cone diameter is for its position at FL2, where the cone has its largest diameter. Since the observed cone diameter is path length dependent, the camera position was fixed for all measurements. The experimental cone diameter was obtained using the CMOS calibration and by fitting the cone with the Radial Profile Plot Java Script in Image-J 1.44p (National Institutes of Health, USA).

The Raman peak amplitude of the 890 cm^{-1} mode of poly(bisphenol A carbonate), 1001 cm^{-1} mode of polystyrene and the 999 cm^{-1} mode of thiophenol was modelled by the sum square electric field (SSEF) generated within the analyte layer. Three-dimensional finite-difference time-domain simulations were used to calculate the SSEF with a Yee cell size of 5 nm, 2000 cycles, a 35.00° to 55.00° angle range and a 0.05° angle resolution. The SSEF calculations that best modelled our experimental Raman peak amplitude measurements used a 785-nm wavelength (i.e., the excitation wavelength). Fresnel reflectivity calculations were performed using IGOR Pro (WaveMetrics, Inc., Lake Oswego, OR) Macros available from Corn *et al.*[46] to model the cone intensity as a function of incident angle. The angle range was set from 0.000° to 90.000° with a 0.009° angle resolution.

Results and Discussion

Directional RS Instrumentation with Self-Assembled Monolayer Sensitivity

Herein, we demonstrate instrumentation that enables the simultaneous collection of the entire surface-plasmon-polariton cone and the Raman scattering as functions of incident angle. It has been pointed out that the collection of the entire cone as a function of incident angle requires a complicated optical setup.[35] Fig. 2 shows a simple optical setup that allows the collection of the cone intensity, cone diameter and directional Raman scattering using a single motorized translational mirror to scan the incident angle. We first test how well the cone properties are modelled for a bare gold film prior to showing self-assembled monolayer sensitivity, as the gold film parameters are used to model the latter (Fig. 3). For a 50-nm gold film, there is good agreement between the calculated incident angle that produces the maximum attenuation of the reflected light (the surface plasmon resonance angle, 35.530°) and the 35.53° experimental incident angle producing the maximum cone intensity (Fig. 3A). The attenuation in the reflected light intensity corresponds to excitation of surface plasmons in the gold film, and the cone is measured at angles where surface plasmons are excited, as expected. Similarly, the experimental cone diameter (Fig. 3B) is 2.639 ± 0.003 cm and the calculated cone diameter from the far-field angular radiation pattern (Fig. 3C) is 2.662 cm (Fig. 3D). The capability of the instrument to image the cone as the incident angle of light is scanned from 0.00° to 60.00° is shown in ESI Fig. S2 and supporting movie.

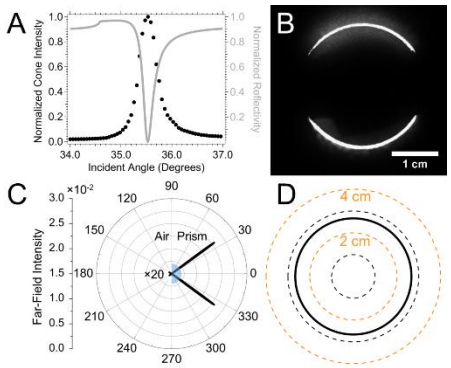

Fig. 3 (A) Experimental cone intensity (dotted symbol) and calculated reflectivity (solid gray line) for prism/50-nm gold/air. (B) Cone acquired at an incident angle of 35.53°. Translational mirrors block the incident light (right) and reflected light (left) from reaching the detector, which is why the cone is not continuous. (C) Calculated far-field angular radiation pattern. The far-field intensity on the air side is multiplied by 20. (D) Calculated cone diameter obtained from the far-field angular radiation pattern projected to the far-field.

The directional RS of a self-assembled monolayer of thiophenol on a smooth planar gold film collected at an incident angle of 35.60°, where the maximum cone intensity is observed, is shown in Fig. 4A. The bands at 999, 1022, 1177, 1470 and 1573 cm^{-1} in Fig. 4A can be assigned to the in-plane ring-breathing mode, in-plane C-H bending mode, in-plane C-H deformation mode, in-plane C-C ring deformation mode, and C-C ring stretching mode, respectively.[47-49] The signal-to-noise ratio of the 999 cm^{-1} Raman mode of thiophenol is 79 when the full Raman signal emanating from the cone is collected for 10 s. McKee *et al.*[39] reported the signal-to-noise ratio of a thiophenol monolayer on a smooth planar gold film to be 6.8 when the Raman signal is collected for 60 s on the sample side in the Kretschmann configuration (using the same laser, spectrometer and detector as shown in Fig. 2). This simple comparison does not take into account some differences in the optics that were used, however, it shows the benefit of collecting the full Raman signal from the surface-plasmon-polariton cone using the instrument shown in Fig. 2. This benefit is credited to the magnitude and directionality of the scattered light at a defined angle on the prism side.

Comparing the bare gold film and the thiophenol monolayer, there is a 0.07° shift in the angle that produces the maximum cone intensity. This shift is consistent with what has been reported in the literature for self-assembled monolayers measured by surface plasmon resonance where the reflectivity minimum is measured.[50-52] Similarly, there is an increase in the cone diameter comparing the bare gold film (2.639 ± 0.003 cm) and the monolayer (2.863 ± 0.005 cm) as shown in Fig. 4B. The increase in the angle that produces the maximum cone intensity and the increase in the cone diameter are attributed to the changes in the local refractive index of the dielectric medium adjacent to the gold film. Both parameters exhibit monolayer sensitivity, and sub-monolayer sensitivity is expected.

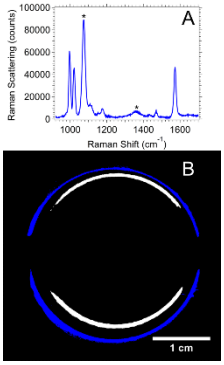

Fig. 4 (A) Directional Raman spectrum of a self-assembled monolayer of thiophenol at a Weierstrass prism/50-nm gold/thiophenol/air interface in the Kretschmann geometry. The acquisition time is 10 s with 3 accumulations using an incident power of 200 mW. The asterisks (*) represent a peak that originates from the sapphire prism. (B) An overlay of the surface-plasmon-polariton cones for (blue) thiophenol self-assembled monolayer and (white) bare gold film acquired at the incident angle producing the maximum cone intensity of 35.60° and 35.53°, respectively.

Quantification and Modelling of the Cone Diameter, Cone Intensity, and Raman Scattering

Polymer films of ~10 to 100-nm thickness were used to quantify the cone intensity and diameter. An image of the overlaid experimental cones for 10 and 50-nm poly(bisphenol A carbonate) films (Fig. 5A) and 30, 60, 70, 80, 90, 100-nm polystyrene films (Fig. 5B) are shown at the incident angle producing the maximum cone intensity, which varies with each sample as discussed below. The calculated cone diameters for poly(bisphenol A carbonate) films (Fig. 5C) and polystyrene films (Fig. 5D) correlate very well with the experimental cone diameters in Fig. 5A and 5B, with an average percent difference of 1%. The emission cone diameter increases with increasing sample thickness due to the increase in the angle of the directionally scattered light through the Weierstrass prism as shown by the calculated far-field angular radiation pattern (ESI Fig. S3). Both the calculated and experimentally measured cone diameter quadratically increase with polymer thickness (Fig. 5E). While the absolute cone diameter is dependent on the system optics, it can be concluded that the cone diameter is sensitive to the thickness of the adsorbate layer (as quantified below).

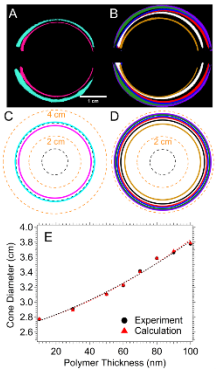

Fig. 5 (A, B) Experimentally measured and (C, D) calculated surface-plasmon-polariton cone for 10 nm (pink), 30 nm (gold), 50 nm (cyan), 60 nm (white/black), 70 nm (red), 80 nm (blue), 90 nm (green) and

100 nm (purple) polymer films. Polymer films are composed of (A, C) poly(bisphenol A carbonate) and (B, D) polystyrene. The experimental and calculated cones have been overlaid for easier comparison. The calculated cone used the polymer thicknesses obtained from profilometry measurements (ESI Fig. 1S). The incident angles at which the experimental cones were collected are 36.00°, 37.45°, 40.15°, 40.94°, 43.59°, 45.76°, 48.00°, and 50.22° for the increasing polymer thicknesses, respectively. The indices of refraction for poly(bisphenol A carbonate) and polystyrene are the same under these experimental conditions. (E) Graphs of experimental (black circle) and calculated (red triangle) cone diameter as a function of polymer thickness. The black dashed line represents a polynomial fit for the experimental data and the red dash line represents a polynomial fit for the calculated data ($y = (2.679\pm0.005) + (0.0067\pm0.0005)x + (0.000047\pm0.000006)x^2$; $R^2 = 0.988$).

Fig. 6A and 6B show the measured cone intensity and calculated reflected light intensity from the interface as a function of incident angle for the polymer samples. As with the calibration plot for the cone diameter (Fig. 5E), the incident angle that produces the maximum cone intensity quadratically increases with polymer thickness (Fig. 6C). SPR-based techniques are inevitably not linear over a broad range of thicknesses or indices of refraction as reported by Corn *et. al.,*[53] although the calibration can be considered linear over a narrow range of thicknesses or indices of refraction. Additionally, the cone intensity as a function of incident angle is well modelled by the calculated surface plasmon resonance angle and is sensitive to sample thickness.

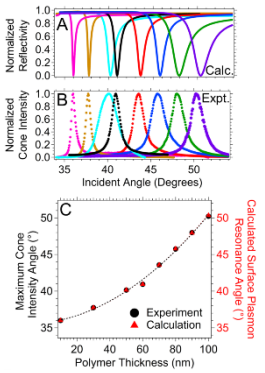

Fig. 6 (A) Calculated angle dependent reflectivity curves and (B) the measured angular dependence of the surface-plasmon-polariton cone intensity for 10 nm (pink), 50 nm (cyan) poly(bisphenol A carbonate) and 30 nm (gold), 60 nm (black), 70 nm (red), 80 nm (blue), 90 nm (green) and 100 nm (purple) polystyrene films. (C) Plot of the measured incident angle that produces the maximum cone intensity (black circle) and the calculated surface plasmon resonance angle using the polymer thickness obtained from profilometry measurements (red triangle). The black dashed line represents a polynomial fit for the experimental data and the red dash line represents a polynomial fit for the calculated data ($y = (35.70\pm0.02) + (0.025\pm0.001)x + (0.00123\pm0.00002)x^2$; $R^2 = 0.998$).

The Raman spectra of 10-nm poly(bisphenol A carbonate) and 100-nm polystyrene films collected at an incident angle that produces the largest signal are shown in ESI Fig. S4. There are only minor differences in the relative intensities of the peaks when comparing the spectra for the bulk powder and the thin films; these minor differences can be explained by the varying spectral background. The directional RS data collected over the full range of incident angles for the poly(bisphenol A

carbonate) (Fig. 7A, C) and polystyrene (Fig. 7B, D, E, F, G, and H) films with varying thicknesses are plotted as their Raman shift versus the incident angle with the color scale representing the Raman scattering intensities.

The 890 cm^{-1} and 995 cm^{-1} peaks assigned to poly(bisphenol A carbonate) have the highest intensity in the angular range from 35.92° to 36.19° for the 10-nm film (Fig. 7A). The 1001 cm^{-1} and 1023 cm^{-1} Raman peaks of polystyrene have the highest intensity in the angular range from 36.03° to 38.78° for the 30-nm film (Fig. 7B). There is also an increase in the background at the angles that produce the maximum Raman scattering. A cross-section of the peak amplitude (solid colored lines) and the calculated sum square electric field as a function of incident angle (dashed gray line) show a good agreement for all the polymer films (Fig. 7I). A quadratic increase in the angle producing the maximum Raman scattering intensity is observed with increasing polymer thickness. Averaging over all the samples, the maximum Raman scattering intensity is measured within 0.5° of the angle producing the maximum cone intensity.

The smallest difference in the adsorbate thickness (i.e., with a ~1.575 index of refraction) that can be measured when considering the limits of the instrument resolution is the same for all three parameters collected on the directional RS instrument and is 0.6 nm. When measuring the cone intensity and Raman scattering, future iterations of the instrumentation can be improved with an angular resolution of 0.001 degrees. The smallest change in the cone diameter that can be measured is 0.4 cm, this parameter could also be improved by other image processing methods and using a camera with a larger sensitive area. Future instrument designs will compare well with standard SPR instrumentation, and of course have the added capability to perform sensitive *in situ* Raman measurements.

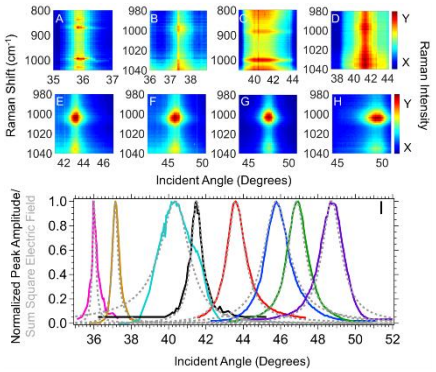

Fig. 7 (A-H) Raman scattering intensity as a function of Raman shift and incident angle on a color amplitude scale. (A, C) Polymer films are composed of 10 and 50-nm thick poly(bisphenol A carbonate) and (B, D, E, F, G, and H) 30, 60, 70, 80, 90, 100-nm polystyrene. The Raman scattering intensity scale in units of counts is designated by X and Y in the color scale, with (A) X,Y = 6,000 to 18,000, (B) X,Y = 80,000 to 120,000, (C) X,Y = 15,000 to 32,000, (D) X,Y = 40,000 to 80,000, (E) X,Y = 15,000 to 30,000, (F and G) X,Y = 10,000 to 20,000, and (H) X,Y = 5,000 to 20,000. (I) Peak amplitude versus incident angle of the 890 cm^{-1} mode of poly(bisphenol A carbonate) and 1001 cm^{-1} mode of polystyrene, (pink) 10 nm, (gold) 30 nm, (cyan) 50 nm, (black) 60 nm, (red) 70 nm, (blue) 80 nm, (green) 90 nm, (purple) 100 nm film (solid line) and the sum square electric field (dashed gray line) calculated using the sample thickness obtained from profilometry measurements. The standard deviation from three replicate experimental measurements is not perceptible on this scale. The acquisition times for the 10 and 50-nm poly(bisphenol A carbonate) films were 180 s and 120 s, respectively. For the 70, 80, 90, and 100-nm

polystyrene films, the Raman spectra were collected for 30 s and for the 30 and 60-nm polystyrene films a 120 s acquisition time was used. All polymer film spectra had 2 accumulations to facilitate cosmic ray removal.

Conclusions

The directional RS method enables the simultaneous collection of the surface-plasmon-polariton cone intensity, cone diameter and Raman scattering as a function of incident angle with a single instrument. The quantitative study of all three parameters using a thiophenol monolayer and thin polymer films as model samples has been presented. Overall, all three measured parameters are well modelled with simple calculations and exhibit a quadratic dependence within a broad range of adsorbate thickness. It is important to note, while the films used to demonstrate the quantitative relationship of each parameter and adsorbate thickness were homogeneous, the multi-parameter directional RS method will be very beneficial for analyzing multicomponent films. For example, the index of refraction, thickness and chemical content of the multicomponent films can be simultaneously measured. The multi-parameter analysis will be useful for smooth films where the film morphology and composition affects its function, such as many films used in energy capture and conversion devices. In addition, the directional Raman signal with the combined measurement of the surface-plasmon-polariton cone will be a useful alternative to surface plasmon resonance spectroscopy when added chemical measurements are beneficial.

"Other Notes" or Competing Financial Interest

The authors declare competing financial interest(s): Stephen C. Weibel has financial interest in the commercial development of this technology.

Acknowledgements

This research was supported by the U.S. Department of Energy, Office of Science, Basic Energy Sciences, Chemical Sciences, Geosciences, and Biosciences Division. The research was performed at the Ames Laboratory, which is operated for the U.S. DOE by Iowa State University under contract # DE-AC02-07CH11358. Profilometry measurements were performed at the Iowa State University W.M. Keck Microfabrication Facility.

Electronic Supplementary Information (ESI)

Thickness of poly(bisphenol A carbonate) and polystyrene films measured by profilometry can be found in supplemental information Fig. S1. Cone images at selected incident angles and a movie (.AVI file) to go along with the cone images can be found in supplemental information Fig. S2. Calculated far-field angular radiation pattern for the cone diameters shown in Fig. 5, can be found in supplemental information Fig. S3. The Raman spectra of 10-nm poly(bisphenol A carbonate) and 100-nm polystyrene films from the data set shown in Fig. 7, can be found in supplemental information Fig. S4.

Notes and References

1. Y. Wang, J. Dostalek and W. Knoll, *Procedia Engineering*, 2010, **5**, 1017-1020.
2. A. Abbas, M. J. Linman and Q. Cheng, *Sensors and actuators. B, Chemical*, 2011, **156**, 169-175.
3. B. Liedberg, C. Nylander and I. Lunström, *Sensors and Actuators*, 1983, **4**, 299-304.
4. L. A. Lyon, M. D. Musick and M. J. Natan, *Analytical Chemistry*, 1998, **70**, 5177-5183.
5. E. A. Smith, W. D. Thomas, L. L. Kiessling and R. M. Corn, *Journal of the American Chemical Society*, 2003, **125**, 6140-6148.
6. J. S. Yuk, G. N. Gibson, J. M. Rice, E. F. Guignon and M. A. Lynes, *Analyst*, 2012, **137**, 2574-2581.
7. J.-F. Masson, *ACS Sensors*, 2017, **2**, 16-30.
8. J. Matsui, K. Akamatsu, N. Hara, D. Miyoshi, H. Nawafune, K. Tamaki and N. Sugimoto, *Analytical Chemistry*, 2005, **77**, 4282-4285.
9. D. A. Woods and C. D. Bain, *Analyst*, 2012, **137**, 35-48.
10. R. Iwamoto, K. Ohta, M. Miya and S. Mima, *Applied Spectroscopy*, 1981, **35**, 584-587.
11. T. Ikeshoji, Y. Ono and T. Mizuno, *Appl. Opt.*, 1973, **12**, 2236-2237.
12. D. A. Beattie, M. L. Larsson and A. R. Holmgren, *Vibrational Spectroscopy*, 2006, **41**, 198-204.
13. C. Chen, L. Dan-Feng, G. Ran, C. Jin and Q. Zhi-Mei, *Applied Physics Express*, 2016, **9**, 062001.
14. R. K. Fisher and R. W. Gould, *Physical Review Letters*, 1969, **22**, 1093-1095.
15. A. Webster and F. Vollmer, *Opt. Lett.*, 2013, **38**, 244-246.
16. M. Futamata, *Appl. Opt.*, 1997, **36**, 364-375.
17. J. Giergiel, C. E. Reed, J. C. Hemminger and S. Ushioda, *The Journal of Physical Chemistry*, 1988, **92**, 5357-5365.
18. W. Wittke, A. Hatta and A. Otto, *Applied Physics A*, 1989, **48**, 289-294.
19. A. J. Braundmeier and H. E. Tomaschke, *Optics Communications*, 1975, **14**, 99-103.
20. N. Calander, *Analytical Chemistry*, 2004, **76**, 2168-2173.
21. C. Chen, D.-F. Lu, R. Gao and Z.-M. Qi, *Optics Communications*, 2016, **367**, 86-94.
22. D. G. Zhang, K. J. Moh and X. C. Yuan, *Opt. Express*, 2010, **18**, 12185-12190.
23. J. S. Yuk, M. Trnavsky, C. McDonagh and B. D. MacCraith, *Biosensors and Bioelectronics*, 2010, **25**, 1344-1349.
24. I. Gryczynski, J. Malicka, K. Nowaczyk, Z. Gryczynski and J. R. Lakowicz, *Thin Solid Films*, 2006, **510**, 15-20.
25. I. Gryczynski, J. Malicka, Z. Gryczynski, K. Nowaczyk and J. R. Lakowicz, *Proceedings of SPIE--the International Society for Optical Engineering*, 2004, **5327**, 37-44.
26. I. Gryczynski, J. Malicka, K. Nowaczyk, Z. Gryczynski and J. R. Lakowicz, *The Journal of Physical Chemistry B*, 2004, **108**, 12073-12083.
27. I. Gryczynski, J. Malicka, J. Lukomska, Z. Gryczynski and J. R. Lakowicz, *Photochemistry and Photobiology*, 2004, **80**, 482-485.
28. S. Byahut and T. E. Furtak, *Review of Scientific Instruments*, 1990, **61**, 27-32.
29. M. Futamata, P. Borthen, J. Thomassen, D. Schumacher and A. Otto, *Applied Spectroscopy*, 1994, **48**, 252-260.
30. M. Futamata, *Langmuir*, 1995, **11**, 3894-3901.
31. M. Futamata, E. Keim, A. Bruckbauer, D. Schumacher and A. Otto, *Applied Surface Science*, 1996, **100**, 60-63.
32. M. Futamata, *The Journal of Physical Chemistry*, 1995, **99**, 11901-11908.
33. H. Li, S. Xu, Y. Liu, Y. Gu and W. Xu, *Thin Solid Films*, 2012, **520**, 6001-6006.

34. S. A. Meyer, B. Auguié, E. C. Le Ru and P. G. Etchegoin, *The Journal of Physical Chemistry A*, 2012, **116**, 1000-1007.
35. S. A. Meyer, E. C. Le Ru and P. G. Etchegoin, *Analytical Chemistry*, 2011, **83**, 2337-2344.
36. S.-X. Huo, Q. Liu, S.-H. Cao, W.-P. Cai, L.-Y. Meng, K.-X. Xie, Y.-Y. Zhai, C. Zong, Z.-L. Yang, B. Ren and Y.-Q. Li, *The Journal of Physical Chemistry Letters*, 2015, **6**, 2015-2019.
37. J. M. Bobbitt, D. Mendivelso-Pérez and E. A. Smith, *Polymer*, 2016, **107**, 82-88.
38. C. A. Damin, V. H. T. Nguyen, A. S. Niyibizi and E. A. Smith, *Analyst*, 2015, **140**, 1955-1964.
39. K. J. McKee, M. W. Meyer and E. A. Smith, *Analytical Chemistry*, 2012, **84**, 4300-4306.
40. K. J. McKee, M. W. Meyer and E. A. Smith, *Analytical Chemistry*, 2012, **84**, 9049-9055.
41. K. J. McKee and E. A. Smith, *Review of Scientific Instruments*, 2010, **81**, 043106.
42. M. W. Meyer, K. L. Larson, R. C. Mahadevapuram, M. D. Lesoine, J. A. Carr, S. Chaudhary and E. A. Smith, *ACS Applied Materials & Interfaces*, 2013, **5**, 8686-8693.
43. M. W. Meyer, K. J. McKee, V. H. T. Nguyen and E. A. Smith, *The Journal of Physical Chemistry C*, 2012, **116**, 24987-24992.
44. M. D. Lesoine, J. M. Bobbitt, S. Zhu, N. Fang and E. A. Smith, *Analytica Chimica Acta*, 2014, **848**, 61-66.
45. J. M. Bobbitt, S. C. Weibel, M. Elshobaki, S. Chaudhary and E. A. Smith, *Analytical Chemistry*, 2014, **86**, 11957-11961.
46. R. M. Corn, 2014.
47. M. A. Bryant, S. L. Joa and J. E. Pemberton, *Langmuir*, 1992, **8**, 753-756.
48. R. Holze, *Physical Chemistry Chemical Physics*, 2015, **17**, 21364-21372.
49. W. K. Yi, C.-W. Park, M.-S. Kim and K. Kim, *Bulletin of the Korean Chemical Society*, 1987, **8**, 291-296.
50. Y. Liu, S. Xu, H. Li, X. Jian and W. Xu, *Chemical Communications*, 2011, **47**, 3784-3786.
51. C. Fu, C. Hu, Y. Liu, S. Xu and W. Xu, *Analytical Methods*, 2012, **4**, 3107-3110.
52. B. P. Nelson, A. G. Frutos, J. M. Brockman and R. M. Corn, *Analytical Chemistry*, 1999, **71**, 3928-3934.
53. A. G. Frutos, S. C. Weibel and R. M. Corn, *Analytical Chemistry*, 1999, **71**, 3935-3940.